HAL open science

Confidence intervals of energies predicted by MODal ENergy Analysis method

Nicolas Totaro, J. L. Guyader

▶ To cite this version:

Nicolas Totaro, J. L. Guyader. Confidence intervals of energies predicted by MODal ENergy Analysis method. Journal of Sound and Vibration, 2021, 509, 10.1016/j.jsv.2021.116229 . hal-03639618

HAL Id: hal-03639618

https://hal.science/hal-03639618v1

Submitted on 13 Apr 2022

HAL is a multi-disciplinary open access archive for the deposit and dissemination of scientific research documents, whether they are published or not. The documents may come from teaching and research institutions in France or abroad, or from public or private research centers.

L'archive ouverte pluridisciplinaire **HAL**, est destinée au dépôt et à la diffusion de documents scientifiques de niveau recherche, publiés ou non, émanant des établissements d'enseignement et de recherche français ou étrangers, des laboratoires publics ou privés.

Journal Pre-proof

Confidence intervals of energies predicted by MODal ENergy Analysis method

N. Totaro, J.L. Guyader

PII: S0022-460X(21)00301-1
DOI: https://doi.org/10.1016/j.jsv.2021.116229
Reference: YJSVI 116229

To appear in: *Journal of Sound and Vibration*

Received date: 18 December 2019
Revised date: 11 May 2021
Accepted date: 23 May 2021

Please cite this article as: N. Totaro, J.L. Guyader, Confidence intervals of energies predicted by MODal ENergy Analysis method, *Journal of Sound and Vibration* (2021), doi: https://doi.org/10.1016/j.jsv.2021.116229

This is a PDF file of an article that has undergone enhancements after acceptance, such as the addition of a cover page and metadata, and formatting for readability, but it is not yet the definitive version of record. This version will undergo additional copyediting, typesetting and review before it is published in its final form, but we are providing this version to give early visibility of the article. Please note that, during the production process, errors may be discovered which could affect the content, and all legal disclaimers that apply to the journal pertain.

© 2021 Published by Elsevier Ltd.

Journal Pre-proof

Confidence intervals of energies predicted by MODal ENergy Analysis method

N. Totaro[a,1], J.L. Guyader[b]

[a] *Univ Lyon, INSA Lyon, LVA EA677, 69621 Villeurbanne, France*
[b] *Sonorhc Technologies, ZA du Vorgey, 01800 Charnoz-sur-Ain, France*

Abstract

MODal ENergy Analysis (MODENA) was previously developed in the same framework as Statistical Energy Analysis (SEA) and Statistical modal Energy distribution Analysis (SmEdA) methods. It deals with energy exchanges between weakly coupled subsystems in vibro-acoustics. However, unlike SEA, MODENA is not a statistical method as it is based on deterministic structures and solved at pure tone. Compared to SmEdA, MODENA takes intrinsically into account couplings between non resonant modes and keeps information about resonance peaks. Consequently, it handles matrices of bigger size than SmEdA with the consequence of higher computation cost.
MODENA was first based on the assumption of uncorrelated forces applied to two coupled oscillators. This assumption was fulfilled by considering a random phase between forces applied to oscillators. In the present article, this assumption is further investigated by considering the phase angle as a random variable with uniform distribution. The expressions for expectation and variance are then derived in this context. They allow estimating confidence intervals of energies predicted by MODENA method. Therefore, even if the assumption of random phase is not fulfilled, the solution should be included in the confidence interval.
It is shown that confidence intervals of energies are rather null in case of two weakly coupled oscillators both excited by forces of equivalent level. The confidence intervals increase at some frequencies when the coupling strength is higher than the critical coupling or when the excitation level difference

[1]Corresponding author. Tel.: + 33172438082. E-mail address: nicolas.totaro@insa-lyon.fr

Journal Pre-proof

Journal Pre-proof

increases.
In case of mutimodal coupling, two numerical test cases are investigated: a plate/cavity case and a cavity/plate/cavity case. In both cases, expectations and variances are computed using MODENA theory and are compared to deterministic responses of the subsystems computed using a finite element software.

Keywords: MODal ENergy Analysis; confidence intervals; energy exchanges

1. Introduction

To tackle the vibro-acoustics challenges of NVH (Noise Vibration Harshness) engineers, different numerical methods are available depending on the frequency range under study. At low to medium frequency, the discretization methods like finite [1] or infinite element methods [2] are well suited. These methods are mainly deterministic and solved in time or frequency. A wide range of applications can be addressed: linear or non-linear systems, multilayered or patterned panels, systems with complex shapes, couplings like joints, bolts, welded points and so on. However, three main issues limit the use of such methods. The first one is due to the size of elements which depends on frequency. The higher the frequency, the smaller the elements. This implies an increase of the number of degrees of freedom and so of the computation time. Second, at medium to high frequency, the variability of system behaviors increases and makes deterministic models unreliable [3]. Third, increasing the number of degrees of freedom makes the analyses difficult and some averaging (by subsystems, by frequency ranges) are often necessary.
At high frequency, alternatives are wave methods [4, 5], radiosity and ray methods [6] and energy methods. Statistical Energy Analysis [7, 8] is the most widely used method to deal with a frequency problem. However, it relies on restrictive assumptions like weak coupling [9] and diffuse field [10]. The results are averaged in space (by subsystems) and often in frequency (by frequency ranges) leading to a highly condensed information. Statistical modal Energy distribution Analysis (SmEdA) [11] is an alternative to SEA when the equipartition of modal energies of subsystems is not reached. This happens when subsystems have neither a naturally diffuse field (light damping) nor forced diffuse field (rain-on-the-roof excitation). SmEdA is frequency

Journal Pre-proof

averaged and only resonant modes in a frequency band are not considered in the computation. As a consequence, non resonant transmission is not taken into account even if it can be represented by indirect coupling in some specific configurations [12]. However, SmEdA provides really useful results and modal energy paths can be evaluated [13].

MODal ENergy Analysis (MODENA) [14] follows the same philosophy as SmEdA but at pure tone. A power balance is set for each mode of a subsystem at each frequency. A modal input power can either be dissipated or exchanged with modes of other coupled subsystems. As in SmEdA, the net exchanged power between to coupled modes is a function of modal energies of both modes. The main difference comes from the fact that MODENA is not frequency averaged. As a result, the coupling coefficients depend on frequency and non resonant transmission is taken into account. In addition, resonance peaks are still visible in the energy frequency responses provided by MODENA. In counterpoint, even if MODENA is based on modes of uncoupled subsystems, the computation time is higher due to the bigger matrix to solve (that takes into account all the modes in the frequency range). MODENA tries to find a trade-off between computation time and relevance of obtained results.

MODENA is derived in the framework of two coupled oscillators. The two main assumptions are weak coupling and uncorrelated forces applied to the oscillators. Zhang *et al.* [15] demonstrated that the MODENA reliability depends on the type of excitations used, the best results being obtained with purely random pressure fields while the worst results are obtained with perfectly correlated pressure fields.

In [14], the assumption of uncorrelated forces was considered achieved in case of forces linked by a random phase. In the present article, it is demonstrated that the expectation of modal energies in case of a random phase is indeed equal to the modal energy considering uncorrelated forces. In addition, an analytical expression of the variance of modal energies is also derived leading to a confidence interval as a function of frequency. It is shown that the variance depends on modal energies of the two coupled oscillators. Expectations and variances are first analyzed in the simple case of two coupled oscillators. Then, multi-modal coupling is investigated through two test cases: a plate coupled to a cavity (the plate being excited by a point force) and a cavity coupled to a plate backed by another cavity (the first cavity being excited by a point source). In both cases, the results are compared to deterministic solutions provided by the ACTRAN commercial software [16].

Journal Pre-proof

However, it is worth mentioning here that MODENA method is not a statistical method as SEA is. Indeed, MODENA assumptions are not based on a population of similar structures. Structures in MODENA are considered deterministic so the variability issue appearing at high frequency can not be tackled by MODENA. The study of confidence interval addressed in the present article should not be compared to expectation and variance analyses treated since decades by many authors [17, 18, 19]. Although the mean energy values of MODENA systems are the same as in SEA-related methods, the underlying statistical model (and indeed the variance) is substantially different, as the only source of randomness is the phase angle between the forces.

MODENA is an approximate solution for weakly coupled vibro-acoustic subsystems where the modal behavior of the uncoupled subsystems is accounted for. In addition, the interaction forces between subsystems are assumed to be uncorrelated. The contribution of the present article is then that it offers a way to estimate errors made in assuming uncorrelated coupling forces in between subsystems.

2. Basics of MODal ENergy Analysis

Consider two oscillators coupled through a gyroscopic coupling as shown in Fig. 1. Each oscillator i ($i = 1, 2$) consists of a mass M_i, a spring k_i and a damper λ_i characterized by a damping bandwidth $\Delta_i = \lambda_i/M_i$. The coupling is of gyroscopic type characterized by $G = \sqrt{M_1 M_2}\gamma$ where γ is the gyroscopic coupling coefficient. Each oscillator i is excited by an external force $F_i(\omega)$, ω being the angular frequency. In [14], forces $F_i(\omega)$ are considered as uncorrelated forces so that cross-spectra $S_{ij}(\omega) = F_i(\omega)F_j^*(\omega) = 0$ ($\bullet^*$ being the complex conjugate). In the following the ω-dependency will be omitted for sake of clarity. According to [14], the total energy E_i of oscillator i coupled to oscillator j is given by

$$E_i = \frac{M_i}{4}(\omega^2 + \omega_i^2)\left[|H_{ii}|^2 S_{ii} + |H_{ij}|^2 S_{jj}\right], \tag{1}$$

and the net exchanged power Π_{ij} between oscillator i and oscillator j ($j \neq i$) is given by

$$\Pi_{ij} = -\frac{1}{2}G\omega^2 \Re\left(H_{ji}^* H_{ii} S_{ii} + H_{jj}^* H_{ij} S_{jj}\right), \tag{2}$$

Journal Pre-proof

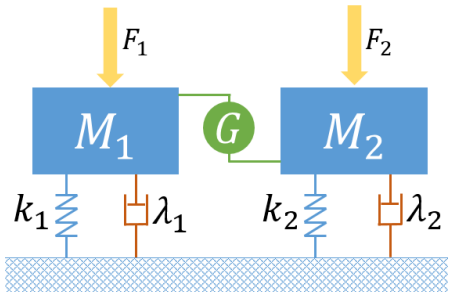

Figure 1: Sketch of two oscillators coupled by a gyroscopic coupling

where $S_{ii} = F_i F_i^*$ (F_i^* being the complex conjugate of F_i) are the force auto-spectra, ω_i are the eigen-frequencies of oscillator i and $\Re$ stands for the real part of a complex number. The terms H_{ij} ($|\bullet|^2 = \bullet\bullet^*$) are transfer functions given by

$$H_{ii} = \frac{1}{M_i} \frac{\omega_j^2 - \omega^2 + \mathrm{i}\omega\Delta_j}{\Sigma_{ij}}, \tag{3}$$

$$H_{ij} = (-1)^j \, \mathrm{i}\omega \frac{\gamma}{\sqrt{M_i M_j}} \frac{1}{\Sigma_{ij}}, \tag{4}$$

where

$$\Sigma_{ij} = \left(\omega_i^2 - \omega^2 + \mathrm{i}\omega\Delta_i\right)\left(\omega_j^2 - \omega^2 + \mathrm{i}\omega\Delta_j\right) - \omega^2\gamma^2. \tag{5}$$

It has been demonstrated in [14] that S_{11} and S_{22} can be expressed as a function of E_1 and E_2 writing Eq. (1) in a matrix form

$$\begin{bmatrix} |H_{11}|^2 & |H_{12}|^2 \\ |H_{21}|^2 & |H_{22}|^2 \end{bmatrix} \begin{Bmatrix} S_{11} \\ S_{22} \end{Bmatrix} = \begin{Bmatrix} \frac{4E_1}{M_1\left(\omega^2+\omega_1^2\right)} \\ \frac{4E_2}{M_2\left(\omega^2+\omega_2^2\right)} \end{Bmatrix} \tag{6}$$

Expressions for S_{11} and S_{22} can be found solving the system of equations Eq. (6). This leads to

$$S_{ii} = \frac{1}{|H_{ii}|^2|H_{jj}|^2 - |H_{ij}|^2|H_{ji}|^2} \left[\frac{4E_i|H_{jj}|^2}{M_i(\omega^2+\omega_i^2)} - \frac{4E_j|H_{ij}|^2}{M_j(\omega^2+\omega_j^2)}\right]. \tag{7}$$

The net exchanged power Π_{ij}, Eq. (2), can be expressed as a function E_i and E_j as

$$\Pi_{ij} = \alpha_{ij}E_i - \alpha_{ji}E_j, \tag{8}$$

Journal Pre-proof

where α_{ij} (ω-dependency omitted) is a coupling coefficient whose expression is

$$\alpha_{ij} = -\frac{2G\omega^2}{M_i\left(\omega^2+\omega_i^2\right)}\frac{\Re\left(H_{ji}^*H_{ii}\right)|H_{jj}|^2 - \Re\left(H_{jj}^*H_{ij}\right)|H_{ji}|^2}{|H_{ii}|^2|H_{jj}|^2 - |H_{ij}|^2|H_{ji}|^2} \tag{9}$$

or, by introducing Eqs. (3) and (4) in Eq. (9)

$$\alpha_{ij} = \frac{2\gamma^2}{\left(1+\frac{\omega_i^2}{\omega^2}\right)}\frac{\Delta_j\omega^2\left((\omega_i^2-\omega^2)^2+\omega^2\Delta_i^2\right)+\omega^4\gamma^2\Delta_i}{\left((\omega_i^2-\omega^2)^2+\omega^2\Delta_i^2\right)\left((\omega_j^2-\omega^2)^2+\omega^2\Delta_j^2\right)-\omega^4\gamma^4}. \tag{10}$$

Eq. (8) is based on the assumption of uncorrelated forces. This means that, in case of correlated or partially correlated forces, Eq. (8) is an approximation. In the following section, an expression for the introduced variance of this equation in case of correlated forces is derived.

3. Expectations and variances

Consider now that forces F_i and F_j are not uncorrelated anymore but linked with a phase relation represented by a phase angle θ between F_i and F_j. Thus, terms $S_{ij} = F_iF_j^*$ in Eq. (1) are

$$S_{ij} = F_iF_j^* = \sqrt{S_{ii}S_{jj}}e^{-\,\mathrm{i}\theta} = \sqrt{S_{ii}S_{jj}}\left(\cos\theta - \,\mathrm{i}\sin\theta\right). \tag{11}$$

Taking into account the correlation between forces F_i and F_j, the total energy of oscillator i is

$$E_i = \frac{M_i}{4}(\omega^2+\omega_i^2)\left[|H_{ii}|^2S_{ii} + |H_{ij}|^2S_{jj} + 2\Re\left(H_{ii}H_{ij}^*F_iF_j^*\right)\right] \tag{12}$$

or, introducing Eq. (11) in Eq. (12),

$$E_i = \frac{M_i}{4}(\omega^2+\omega_i^2)\left[|H_{ii}|^2S_{ii} + |H_{ij}|^2S_{jj} + 2\sqrt{S_{ii}S_{jj}}\Re\left(H_{ii}H_{ij}^*e^{(-1)^i\,\mathrm{i}\theta}\right)\right]. \tag{13}$$

Expectation $\mu(E_i)$ and variance $\sigma^2(E_i)$ of total energy of oscillator i are

$$\mu(E_i) = \frac{1}{2\pi}\int_0^{2\pi} E_ip(\theta)\,\mathrm{d}\theta \tag{14}$$

and

$$\sigma^2(E_i) = \frac{1}{2\pi}\int_0^{2\pi}(E_i)^2\,p(\theta)\,\mathrm{d}\theta - \mu(E_i)^2. \tag{15}$$

Journal Pre-proof

where $p(\theta)$ is the probability density function of θ. Considering that no *a priori* information can be defined for the probability density function, θ can be chosen as a uniformly distributed random variable so that $p(\theta) = 1$ between 0 and 2π. Assuming this probability density function, $\mu(E_i)$ and $\sigma^2(E_i)$ write

$$\mu(E_i) = \frac{M_i}{4}(\omega^2 + \omega_i^2)\left[|H_{ii}|^2 S_{ii} + |H_{ij}|^2 S_{jj}\right] \tag{16}$$

and

$$\sigma^2(E_i) = \frac{M_i^2}{8} S_{ii} S_{jj} (\omega^2 + \omega_i^2)^2 |H_{ii} H_{ij}^*|^2 \tag{17}$$

As can be seen, Eq. (16) equals Eq. (1). This means that the expectation of E_i when considering a random phase relation between forces F_i is exactly equal to the response of the system under uncorrelated excitations.
Solving the system of equations (6) and introducing expressions of S_{ii} and S_{jj} in Eq. (17), the variance $\sigma^2(E_i)$ of total energy of oscillator i coupled to oscillator j ($i \neq j$) can be written

$$\sigma^2(E_i) = A_{ij}\left(B_i \mu(E_i)^2 + B_j \mu(E_j)^2 + C_{ij}\mu(E_i)\mu(E_j)\right) \tag{18}$$

where

$$A_{ij} = \frac{2\omega^2\gamma^2\left(\omega^2 + \omega_i^2\right)^2\left((\omega_j^2 - \omega^2)^2 + \omega^2\Delta_j^2\right)}{\left(\left((\omega_i^2 - \omega^2)^2 + \omega^2\Delta_i^2\right)\left((\omega_j^2 - \omega^2)^2 + \omega^2\Delta_j^2\right) - \omega^4\gamma^4\right)^2}, \tag{19}$$

$$B_i = -\omega^2\gamma^2 \frac{\left((\omega_i^2 - \omega^2)^2 + \omega^2\Delta_i^2\right)}{(\omega^2 + \omega_i^2)^2}, \tag{20}$$

and

$$C_{ij} = \frac{\left((\omega_i^2 - \omega^2)^2 + \omega^2\Delta_i^2\right)\left((\omega_j^2 - \omega^2)^2 + \omega^2\Delta_j^2\right) + \omega^4\gamma^4}{(\omega^2 + \omega_i^2)(\omega^2 + \omega_j^2)}. \tag{21}$$

It is worth noting that variance $\sigma^2(E_i)$ not only depends on the expectation of total energy of oscillator i but also on the expectation of total energy of oscillator j to which it is coupled.

4. Example of two coupled oscillators

Consider two oscillators coupled through a gyroscopic coupling as sketched in Fig. 1. The characteristics of each oscillator are listed in Tab. 1. Consider three different scenarios:

Journal Pre-proof

	oscillator 1	oscillator 2
mass M_i [kg]	0.01	0.03
stiffness K_i [Nm^{-1}]	6.3165×10^4	4.2637×10^5
damping ratio η_i [-]	0.01	0.01
Eigen-frequency f_i [Hz]	400	600
Force amplitude $\lvert F_i \rvert$ [N] case 1	1	1
case 2	1	0.01
case 3	1	1
coupling coefficient γ [s^{-1}] case 1	1	
case 2	1	
case 3	500	

Table 1: Characteristics of the two coupled oscillators. Three different cases of force amplitudes and coupling coefficients are considered.

- Case 1: weakly coupled oscillators (according to the critical coupling Eq. (22)). Identical force amplitudes $|F_1| = |F_2|$. This case corresponds to, for instance, a mode of a plate coupled to a mode of a cavity, considering that both subsystems are directly excited.
- Case 2: weakly coupled oscillators (according to the critical coupling Eq. (22)). Force amplitude applied on oscillator 1 much higher than the one applied to oscillator 2: $|F_1| = 100|F_2|$. This case corresponds to, for instance, a mode of a plate coupled to a mode of a cavity, considering that only the plate is directly excited. In that example, the "mode of the cavity" is indirectly excited by another mode of the plate, the level of excitation being much lower due to the weak coupling.
- Case 3: strongly coupled oscillators (according to the critical coupling Eq. (22)). Identical force amplitudes $|F_1| = |F_2|$. This case corresponds to an "anti-thermodynamic" behaviour as described in [14].

The critical coupling delimiting a "thermodynamic" and an "anti-thermodynamic" behaviour is defined as

$$\gamma^{\text{crit}} = \sqrt[4]{\left(\frac{(\omega_1^2 - \omega^2)^2}{\omega^2} + \Delta_1^2\right)\left(\frac{(\omega_2^2 - \omega^2)^2}{\omega^2} + \Delta_2^2\right)} \tag{22}$$

The critical coefficient is plotted in Fig. 2 and compared to the coupling coefficients of cases 1 to 3. The coupling coefficients of cases 1 and 2 are much

Journal Pre-proof

lower than the critical coefficient on the whole frequency band ([0;1000]Hz). In case 3, the coupling coefficient is higher than the critical coefficient in two frequency bands around the two eigen-frequencies of the oscillators.

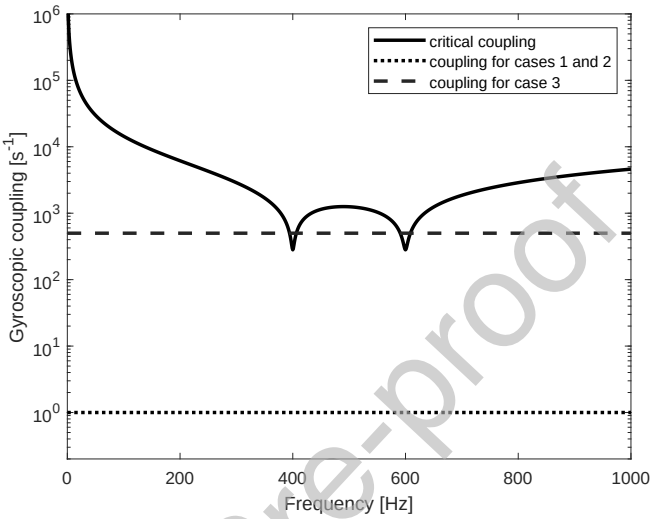

Figure 2: Critical gyroscopic coupling γ^{crit} between oscillators described in Tab. 1 compared to coupling coefficients of cases 1 to 3.

4.1. Weakly coupled oscillators

Both cases 1 and 2 described in Tab. 1 involve weakly coupled oscillators ($\gamma = 1 << \gamma^{\text{crit}}$). The only difference between these two cases lays in the force amplitude $|F_2|$. In case 1, $|F_2| = |F_1|$. In case 2, $|F_2|$ is a hundred times lower than $|F_1|$.

In case 1, Fig. 3 plots the total energies of oscillators 1 and 2. In these figures, 100 random draws for the phase angle between forces F_1 and F_2 have been simulated. The energy expectation computed using Eq. (16) is compared to the average of the random draws (population average) and to each individual random draw. Three confidence intervals obtained from Eq. (18) are also plotted for three different levels (+/-σ, +/-2σ, +/-3σ, where $\sigma = \sqrt{\sigma^2(E_i)}$ is the standard deviation). In case 1, each of the 100 random draws are superimposed either for oscillator 1 or oscillator 2. In this scenario, each oscillator is mainly driven by the external forces F_i and the influence of the other oscillator on its frequency response is negligible. It's a favorable

Journal Pre-proof

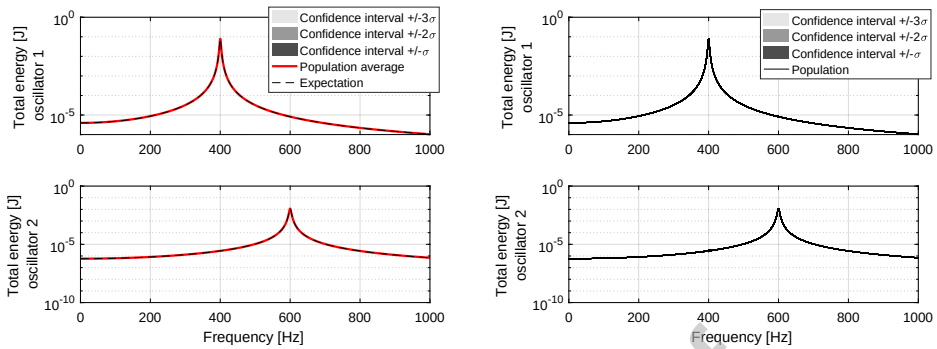

Figure 3: Total energy of oscillators in case of two weakly coupled oscillators excited by forces $|F_1| = |F_2|$. Top figures: oscillator 1; bottom figures: oscillator 2. Left: total energy averaged on 100 random draws of the phase angle, MODENA expectation and confidence intervals. Right: total energies of all the draws and confidence intervals.

case where MODENA expectation is equal to the response of any of the 100 random draws and the energy variance is almost null (not visible in Fig. 3). One can only notice a slight variation of the response of the 100 responses of oscillator 2 at the Eigen-frequency of oscillator 1.
This phenomenon is amplified in case 2 for which $|F_2|$ is much lower than $|F_1|$. As can be seen in Fig. 4, for oscillator 2, a peak appears at the Eigen-frequency of oscillator 1. In this frequency band around 400 Hz, the 100 random draws exhibit a high variation well described by the confidence intervals. The total energy of oscillator 1 is not affected by the presence of oscillator 2 and this leads to an almost null variance.

As predicted, the energy expectation is equal to the average on the 100 random draws. The latter would be equal to the response of the two oscillators excited by uncorrelated forces. In case of perfectly correlated forces, the total energies of both oscillators lie in the confidence interval. This means that, for oscillator 2, the exact value of the total energy is not known in the frequency band around 400 Hz. Nevertheless, the confidence interval is only important for low levels that are highly sensitive to the coupling and is thin on the peaks. This particularity will be advantageous when dealing with a set of modes coupled to another set of modes as presented in section 6.

4.2. Strongly coupled oscillators

Case 3 concerns two strongly coupled oscillators. It is equivalent to case 1 ($|F_1| = |F_2|$) but the coupling coefficient is 500 times higher so that it

Journal Pre-proof

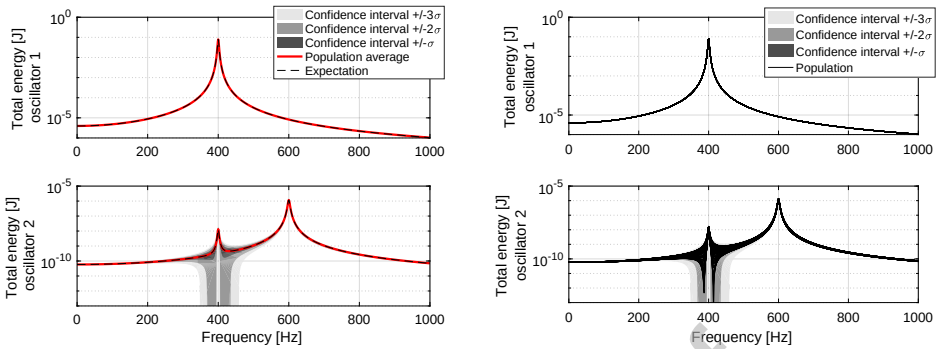

Figure 4: Total energy of oscillators in case of two weakly coupled oscillators excited by forces $|F_1| = 100|F_2|$. Top figures: oscillator 1; bottom figures: oscillator 2. Left: total energy averaged on 100 random draws of the phase angle, MODENA expectation and confidence intervals. Right: total energies of all the draws and confidence intervals.

sometimes exceeds the critical coefficient as shown in Fig. 2. The effect of the strong coupling is clearly visible in Fig. 5: the total energy of oscillator 1 is modified by the presence of oscillator 2. The Eigen-frequency of oscillator 2 generates a peak on the total energy of oscillator 1. Conversely, the total energy of oscillator 2 is modified by the presence of oscillator 1. The variance

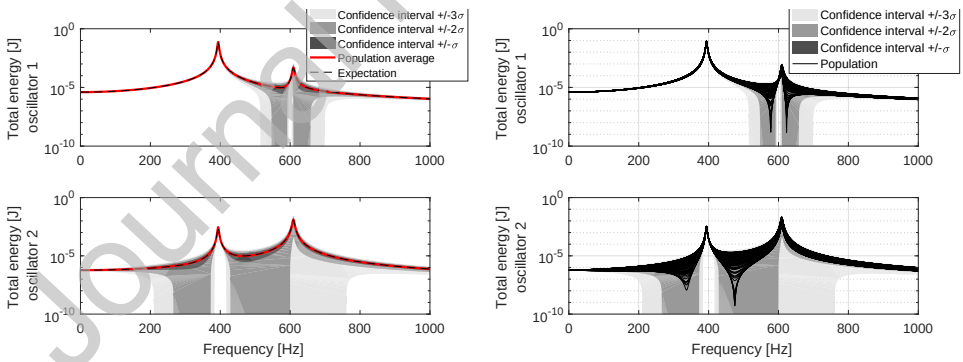

Figure 5: Total energy of oscillators in case of two strongly coupled oscillators excited by forces $|F_1| = |F_2|$. Top figures: oscillator 1; bottom figures: oscillator 2. Left: total energy averaged on 100 random draws of the phase angle, MODENA expectation and confidence intervals. Right: total energies of all the draws and confidence intervals.

of total energy of oscillator 1 is not negligible anymore in the frequency band around the Eigen-frequency of oscillator 2 especially for low levels of energy. The strong interaction between the two oscillators generates a high variability

Journal Pre-proof

in this region. Oscillator 2 is much more subjected to variability due to a higher mass.

5. Extension to multi-modal coupling

5.1. Power balance and modal energies

According to [14], the basic principle governing the energy exchanged between two oscillators can be extended to multi-modal systems. Consider two sets of modes N_p and N_q representing two coupled continuous subsystems as presented in Fig. 6.

In case of a weak coupling between sets of modes (individual couplings

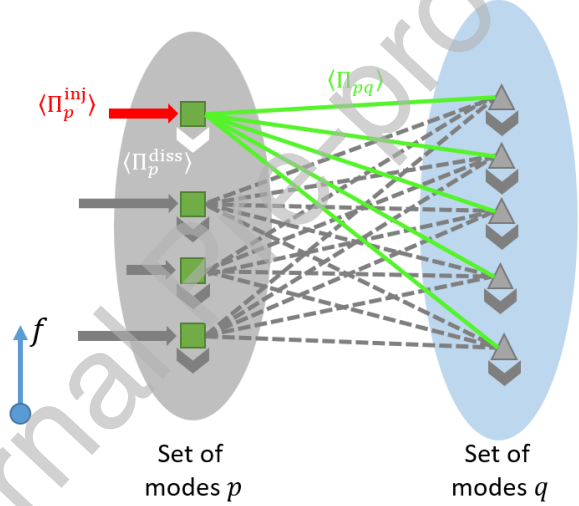

Figure 6: Coupling between two sets of modes

between couple of modes lower that the critical gyroscopic coupling [14]), it has been demonstrated that the power balance for an isolated mode p of the set of modes N_p can be expressed as

$$\mu(\Pi_p^{\text{inj}}) = \mu(\Pi_p^{\text{diss}}) + \sum_q \alpha_{pq}\mu(E_p) - \sum_q \alpha_{qp}\mu(E_q). \tag{23}$$

The modal injected power Π_p^{inj} is either dissipated by the modal damping loss factor or exchanged with the set of modes N_q. Coefficients α_{pq} are modal

Journal Pre-proof

coupling loss factors at pure tone. Knowing modal injected powers and expressing modal dissipated powers as a function of modal energies, one can compute the total modal energy of all modes of both sets of modes.
As presented in previous section, the variance can be deduced from modal energies and information like eigen-frequencies, modal damping and gyroscopic coefficients. Consider, as presented in Fig. 6, the coupling between one mode p of the set of modes N_p and one mode q of the set of modes N_q. Mode p as well as all modes of set of modes N_q are excited by modal forces. Every couple of modes p and q are excited by modal forces F_p and F_q having a random phase θ_{pq}. According to section 3, one can define the variance $\sigma_q^2(E_p)$ due to the coupling between mode p and a particular mode q of the set of modes N_q. The expression of this variance is given by Eq. (18) replacing i by p and j by q.
Assuming that all the phase angles θ_{pq} are independent random variables, the variance $\sigma^2(E_p)$ due to the coupling between one mode p and a set of modes N_q writes

$$\sigma^2(E_p) = \sum_{q=1}^{N_q} \sigma_q^2(E_p) \tag{24}$$

This assumption is done because there is no coupling between modes of the same subsystem and because coupling between modes of two subsystems is weak. Finally, the expectation and variance of the global energy of the set of modes N_p are

$$\mu(E_{N_p}) = \sum_{p=1}^{N_p} \mu(E_p) \tag{25}$$

$$\sigma^2(E_{N_p}) = \sum_{p=1}^{N_p} \sigma^2(E_{p,N_q}) = \sum_{p=1}^{N_p} \sum_{q=1}^{N_q} \sigma_q^2(E_p) \tag{26}$$

5.2. Dissipated power

The expectation of power dissipated by a mode p is given by

$$\mu(\Pi_p^{\text{diss}}) = C_{\eta,p}\mu(E_p) \tag{27}$$

where

$$C_{\eta,p} = \frac{2\eta_{\text{ visc}}\omega_p}{1 + \frac{\omega_p^2}{\omega^2}}, \tag{28}$$

Journal Pre-proof

for a viscous damping η_{visc} and

$$C_{\eta,p} = 2\eta_{\text{struc}}\omega\frac{1}{1+\frac{\omega^2}{\omega_p^2}}, \tag{29}$$

for a structural damping η_{struc}. The variance of power dissipated by a mode p is then given by

$$\sigma^2(\Pi_p^{\text{diss}}) = C_{\eta,p}^2\sigma^2(E_p) \tag{30}$$

Finally, the expectation and variance of power dissipated by a set of modes p (power dissipated by the subsystem) are

$$\mu(\Pi_{N_p}^{\text{diss}}) = \sum_{p=1}^{N_p} C_{\eta,p}\mu(E_p), \tag{31}$$

and

$$\sigma^2(\Pi_{N_p}^{\text{diss}}) = \sum_{p=1}^{N_p} C_{\eta,p}^2\sigma^2(E_p) \tag{32}$$

5.3. Net exchanged power

The expectation of net exchanged power between a mode p and a mode q is

$$\mu(\Pi_{p\leftrightarrow q}) = \alpha_{pq}\mu(E_p) - \alpha_{qp}\mu(E_q), \tag{33}$$

and the variance is

$$\sigma^2(\Pi_{p\leftrightarrow q}) = \alpha_{pq}^2\sigma^2(E_p) + \alpha_{qp}^2\sigma^2(E_q). \tag{34}$$

Finally, the expectation and variance of net exchanged power between a set of modes p and a set of modes q are

$$\mu(\Pi_{N_p\leftrightarrow N_q}) = \sum_{p=1}^{N_p}\sum_{q=1}^{N_q}\mu(\Pi_{p\leftrightarrow q}), \tag{35}$$

and

$$\sigma^2(\Pi_{N_p\leftrightarrow N_q}) = \sum_{p=1}^{N_p}\sum_{q=1}^{N_q}\sigma^2(\Pi_{p\leftrightarrow q}). \tag{36}$$

Journal Pre-proof

6. Numerical validations for multi-modal coupling

Consider two different examples of multi-modal coupling. These two examples consist in weakly coupled subsystems, i.e. cavities filled with air coupled to structures. In the first example, a plate is coupled to a cavity filled with air. As illustrated in Fig. 7(a), the plate is excited by a unit point force. In the second example, a cavity is coupled to a plate coupled itself to another cavity. As shown in Fig. 7(b), one of the cavities is excited by a unit monopole source. The characteristics of the plate and the cavities are listed in Tab. 2.

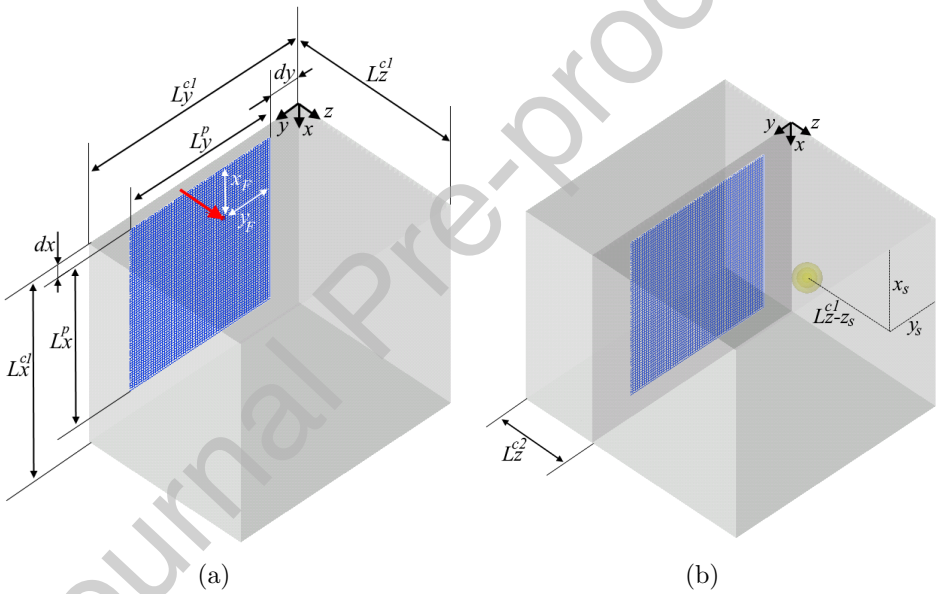

Figure 7: (a) Sketch of Plate/Cavity 1 coupling test case. The plate is excited by a point force at (x_F, y_F). (b) Sketch of the Cavity 2/Plate/Cavity 1 test case. Cavity 1 is excited by a spherical source located at (x_S, y_S, z_S).

In both examples, mode shapes of the plate with simply supported boundary conditions and of the cavities with rigid walls have been computed using analytical solutions up to 3500 Hz. Coupling coefficients α_{pq} have been computed with Eq. (10) and the gyroscopic coefficient γ_{pq} have been computed with Eq. (39) of [14].

	Plate
L_x^p [m]	0.65
L_y^p [m]	0.6
dx [m]	0.0554
dy [m]	0.1254
E_p [Pa]	2e11
ρ_p [kg/m^3]	7800
ν_p [-]	0.3
h_p [mm]	3
η_p^{visc} [-]	0.05
x_F [m]	0.2
y_F [m]	0.2

	Cavity 1	Cavity 2
L_x^c [m]	0.8	
L_y^c [m]	0.9	
L_z^c [m]	0.65	0.3
ρ_c [kg/m^3]	1.2	
c_c [m/s]	340	
η_c^{visc} [-]	0.02	
x_S [m]	0.34	/
y_S [m]	0.22	/
z_S [m]	0.29	/

Table 2: Characteristics of subsystems for the Plate/Cavity 1 and Cavity 2/Plate/Cavity 1 test cases

6.1. Plate/Cavity 1 coupling test case

For the plate/cavity 1 coupling case, the expectations of subsystem energies are plotted in Fig. 8. They are compared to a reference computation made with the commercial finite element software ACTRAN. It is worth mentioning that Actran computation is here completely deterministic: there is no randomness neither in the description of the source nor in the behavior of the subsystems. For the plate energy, the comparison with the reference computation is almost perfect due to the fact that the plate is directly driven by the point force. For the cavity energy, the comparison exhibits the same trends for both curves but some discrepancies are visible. These discrepancies might originate from the uncorrelated forces assumption made in MODENA.

Expectations and confidence intervals are plotted in Fig. 9. Confidence intervals are defined respectively as the expectation plus or minus one, two or three times the standard deviation (square root of the variance).

As can be seen in Fig. 9(a-b), the confidence intervals of the energy of the plate are almost not distinguishable. For the plate, the uncorrelated force assumption is verified (mode shapes of the plate are orthogonal and forces due to the cavity interactions are negligible due to the weak coupling). This point was also observed by Zhang *et al.* [15]. In contrast, the confidence intervals of the cavity energy are clearly visible in Fig. 9(c-d). They translate the fact that, from the cavity point of view, the forces due to the

Journal Pre-proof

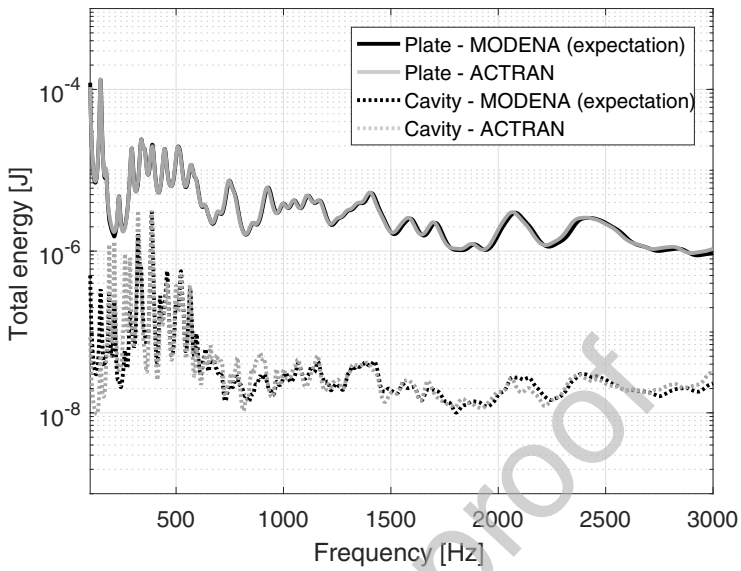

Figure 8: Expectations of the total energies of the plate (solid lines) and the cavity 1 (dotted lines). MODENA expectations: black lines; ACTRAN reference computation: grey lines.

coupling with the plate are not uncorrelated. However, when comparing to the reference computation, one can see that in the whole frequency range, the reference solution always lies in the confidence interval. In addition, as underlined by Zhang *et al.* [15], this kind of excitation is the worst situation for application of MODENA. Indeed, the excitation pressure field is perfectly correlated. It has been demonstrated that MODENA produces much more reliable results in case of rain-on-the-roof excitation (purely random pressure field) or Turbulent Boundary Layer excitations.

6.2. Cavity 2/Plate/Cavity 1 coupling test case

Consider now the same configuration as previously (plate 1 coupled to cavity described in Tab. 2) but with an additional cavity (cavity 2) backing the plate on its other side. Characteristics of this second cavity are listed in Tab. 2. A monopole source is acting in cavity 1 at position $(0.34; 0.22; 0.29)$ m. In that case, two subsystems (the plate and cavity 2) are not directly excited. In addition, cavity 2 is not directly linked to cavity 1. One can expect in that case some huge confidence intervals for the energy of cavity 2. The expectations and confidence intervals for cavity 1, plate and cavity 2

Journal Pre-proof

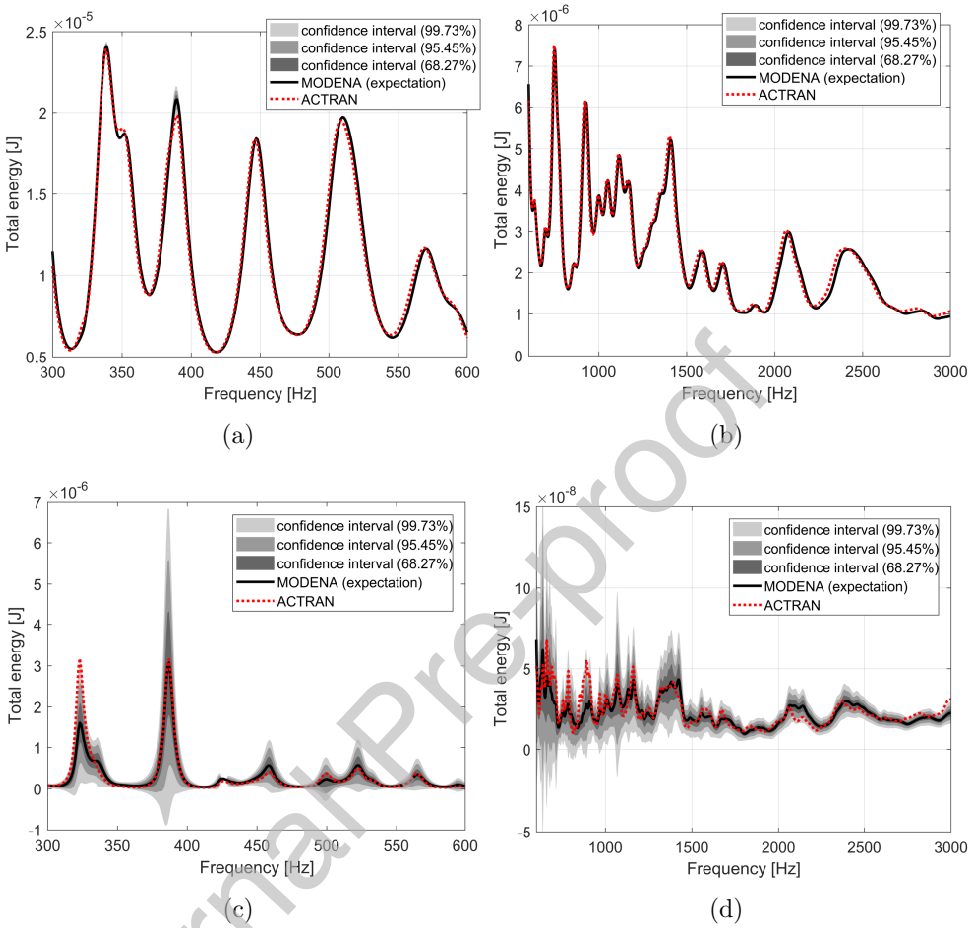

Figure 9: Expectations (solid black lines) and confidence interval (in grey scale) of the total energies of the plate and the cavity. (a): total energy of the plate in the [300:600]Hz frequency range; (b): total energy of the plate in the [600:3000]Hz frequency range; (c): total energy of the cavity in the [300:600]Hz frequency range; (d): total energy of the cavity in the [600:3000]Hz frequency range. Red dotted lines: ACTRAN reference computations.

are plotted in Fig. 10. Again, for the excited subsystem (here cavity 1), the variance of the energy is almost null and the MODENA expectation compares well with simulations. This example is comparable to case 2 of section 4.1: modes of cavity 1 are directly excited and weakly coupled to a set of modes (of the plate) with a low level of excitation (indirect excitation). In that scenario, the response of the excited subsystem is almost unaffected by the

Journal Pre-proof

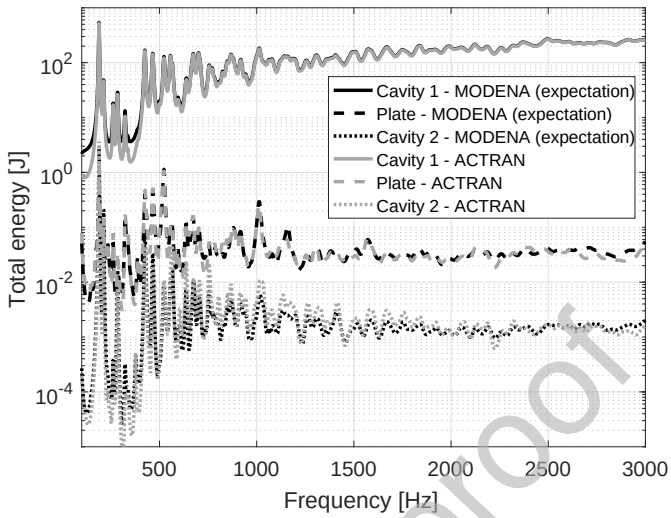

Figure 10: Expectations of the total energies of the cavity 1 (solid lines), the plate (dashed lines) and the cavity 2 (dotted lines). MODENA expectations: black lines; ACTRAN reference computation: grey lines.

presence of the other subsystems and its variability remains low. For the second subsystem (here the plate), the three main peaks in between 400 and 550 Hz (Fig. 11) are due to resonances in cavity 1. This is comparable to case 2 where a peak is due to the Eigen-frequency of the directly excited oscillator generating a relatively high variability of the response around the peak (see Fig. 4). Thus in the [400;550] Hz frequency band, the large confidence intervals (for low levels of energy) are due to this phenomenon. It's the same for the last subsystem (cavity 2) but amplified by the high variance of the energy response of the plate.
At higher frequency, the confidence intervals seems to be lower and spread over the whole frequency response (for low and higher levels) due to the increase of modal overlap. Finally, with respect to the expectations of the energies, the confidence intervals increase from the subsystem closest to the excitation (cavity 1) to the farthest (cavity 2).

6.3. Lateral car window coupled to a passenger compartment

In this example, a lateral car window is coupled to the passenger compartment. The window is made of glass ($E_w = 48.5$ GPa, $\rho_w = 2500$ kg.m^{-3}, $\nu_w = 0.24$, $\eta_w = 0.01$) and is 3 mm thick and has a surface of 0.28 m^2. A

rubber seal ($E_r = 60$ MPa, $\rho_r = 1010$ kg.m^{-3}, $\nu_r = 0{,}48$) is considered glued on the boundaries of the window. The opposite surface of the rubber seal is considered here to be blocked. Both the glazing and the rubber seal have been modeled by solid elements. In the [0:2250] Hz frequency band, the window has 59 Eigen-frequencies. The window is excited by a pressure field due to a turbulent flow around the rear view mirror. An example of the pressure map at a particular frequency can be seen in Fig. 12. The modal input powers are computed with Eq. (37)

$$\Pi_n(\omega) = \frac{1}{2}\Re\left(\int_{S_w} p(M,\omega)V_n^*(M,\omega)\,\mathrm{d}S\right), \tag{37}$$

where $p(M,\omega)$ is the turbulent pressure field and $V_n^*(M,\omega)$ is the normal velocity of mode n of the window at angular frequency ω ($\bullet^*$ stands for the complex conjugate of $\bullet$).
The passenger compartment has a volume of 3.3 m^3 and is filled of air (characteristics of air given in Tab. 2, η_{pc}=0.01). To extract the mode shapes of the acoustic volume, rigid walls boundary conditions have been specified. The acoustic volume has 4950 modes in the [0:2250] Hz frequency band.
The total energy of the passenger compartment is computed in between 300 Hz and 2000 Hz (frequency step 2 Hz). The total energy alongside with the corresponding confidence intervals are plotted in Fig. 13.

As can be seen in Fig. 13, the confidence intervals are much more pronounced at low frequency. Increasing the frequency, the confidence intervals narrow when correlation lengths of the pressure field decrease. As demonstrated by Zhang *et al.*, the accuracy of MODENA strongly depends on the spatial correlation of the pressure field. Therefore, turbulent pressure fields are good candidates for MODENA applications. This translates to small confidence intervals.

Journal Pre-proof

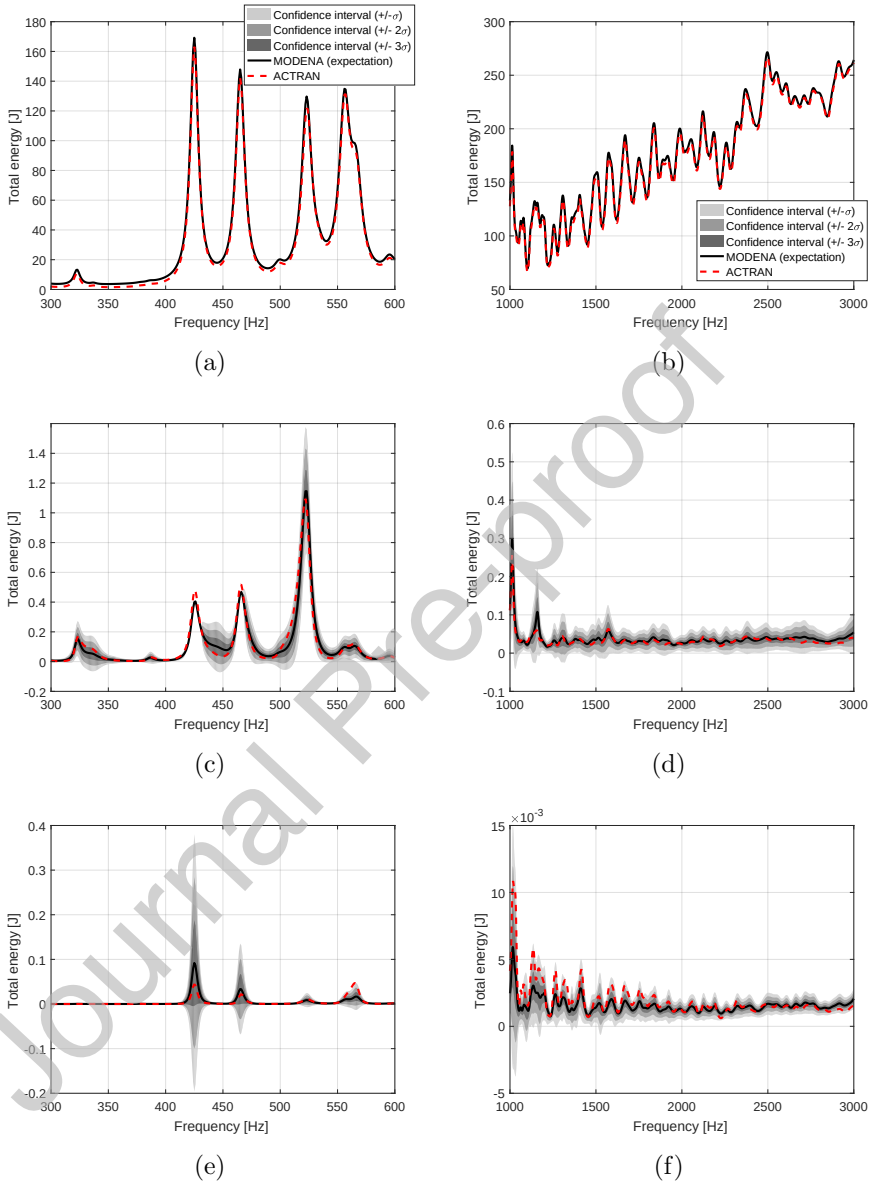

Figure 11: Expectations (solid black lines) and confidence intervals (in grey scale) of the total energies of the subsystems in the Cavity/Plate/Cavity coupling case for two frequency ranges : [300:600]Hz for (a), (c) and (e) and [1000-3000]Hz for (b), (d) and (f). (a) and (b): total energy of Cavity 1; (c) and (d): total energy of the Plate; (e) and (f): total energy of the Cavity 2. Red dotted lines: ACTRAN reference computations.

Journal Pre-proof

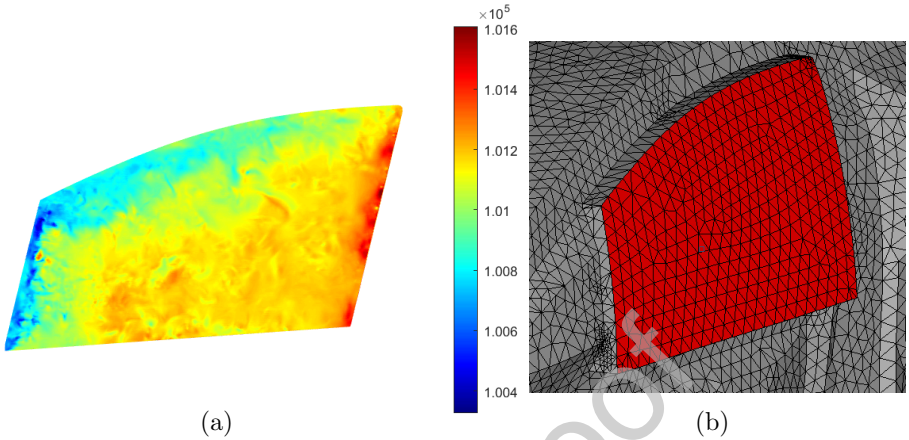

(a) (b)

Figure 12: (a) A lateral car window submitted to a pressure field [Pa] due to a flow around the rear view mirror. (b) Part of the mesh of the passenger compartment and representation (in red) of the coupling surface between the window and the acoustic volume.

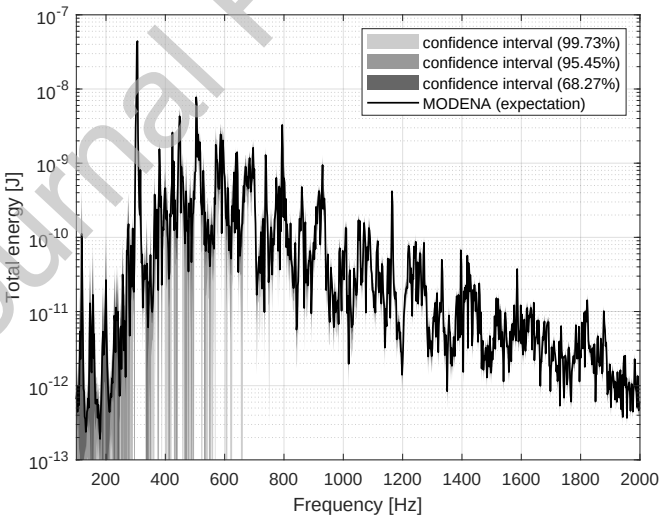

Figure 13: Expectations (black solid line) and confidence intervals (in grey scale) of the total energy of the passenger compartment as a function of frequency.

Journal Pre-proof

Journal Pre-proof

7. Conclusion

The present article has investigated the assumption of uncorrelated forces needed to derive the basic equations of MODal ENergy Analysis. It has been demonstrated that expectations and variances of modal energies can be expressed as a function of modal energies and coefficients depending on frequency and on modal parameters of uncoupled subdomains. The effect of coupling strength on modal energy variances has been analyzed in case of two coupled oscillators. Finally, two cases of multi-modal coupling have been addressed and compared to a reference deterministic solution. For the excited subsystem, the variance is almost null and the expectation almost equal to the deterministic solution. For non directly excited subsystems, the variance increases but the deterministic solution still lies in the MODENA confidence intervals. Finally, it has been observed that an increase of the modal overlap decrease the variance of the subsystems energies.

Acknowledgements

This work was performed within the framework of the Labex CeLyA of Universit de Lyon, operated by the French National Research Agency (ANR-10-LABX-0060/ ANR-11-IDEX-0007).

References

[1] N. Atalla, F. Sgard, Finite element and boudary methods in structural acoustics and vibration, Boca Raton, US: CRC Press (2015).

[2] L. Cremers, K.R. Fyfe, J.P. Coyette, A variable order infinite acoustic wave envelope element, J. Sound. Vib. 171(4) (1994) 483-508.

[3] A. Cicirello, R.S. Langley, The vibro-acoustic analysis of built-up systems using a hybridmethod with parametric and non-parametric uncertainties, J. Sound. Vib. 332 (2013) 2165-2178.

[4] Deckers E., Atak O., Coox L., DAmico R., Devriendt H., Jonckheere S., Koo K., Pluymers B., Vandepitte D., Desmet W., The wave based method: An overview of 15 years of research, Wave Motion 51(4) (2014) 550-565.

Journal Pre-proof

[5] Riou H., Ladevze P., Kovalevsky L., The Variational Theory of Complex Rays: An answer to the resolution of mid-frequency 3D engineering problems, J. Sound. Vib. 332(8) (2013) 1947-1960.

[6] Le Bot A., Sadoulet-Reboul E., High frequency vibroacoustics: A radiative transfer equation and radiosity based approach, Wave motion 51(4) (2014) 598-605.

[7] Lyon R.H., DeJong R., Theory and application of statistical energy analysis, Boston, MA: Butterworth-Heinemann (1995).

[8] Le Bot A., Foundation of statistical energy analysis in vibroacoustics, Oxford, UK: Oxford University Press (2015).

[9] Lafont T., Totaro N., Le Bot A., Review of statistical energy analysis hypotheses in vibroacoustics, Proc. R. Soc. A 470 (2014) 20130515.

[10] Lafont T., Totaro N., Le Bot A., Coupling strength assumption in statistical energy analysis, Proc. R. Soc. A 473 (2017) 20160927.

[11] Maxit L., Guyader J.L., Extension of SEA model to subsystems with non-uniform modal energy distribution, J. Sound. Vib. 265(2) (2003) 337-358.

[12] Maxit L., Ege K., Totaro N., Guyader J.L., Non resonant transmission modelling with statistical modal energy distribution analysis, J. Sound. Vib. 333 (2014) 499-519.

[13] Aragons ., Maxit L., Guasch O., A graph theory approach to identify resonant and non-resonant transmission paths in statistical modal energy distribution analysis, J. Sound. Vib. 350 (2015) 91-110.

[14] Totaro N., Guyader J.L., MODal ENergy Analysis, J. Sound. Vib. 332 (2013) 3735-3749.

[15] Zhang P., Fei Q., Li Y., Wu S., Chen Q., MODal ENergy Analysis for mechanical systems excited by spatially correlated loads, Mech. Syst. Sig. Process. 111 (2018) 362-375.

[16] Free Field Technologies SA, Actran 19.1 Users Guide - Volume 1, Installation, Operations, Theory and Utilities, 2019.

Journal Pre-proof

Journal Pre-proof

[17] Langley R. S., Cotoni V., Response variance prediction in the statistical energy analysis of built-up systems, J. Ac. Soc. Am. 115 (2004) 706-718.

[18] Cotoni V., Langley R. S., Numerical and experimental validation of variance prediction in the statistical energy analysis of built-up systems, J. Sound. Vib. 288(3) (2005) 701-728.

[19] Ji L., Mace B. R., Statistical energy analysis modelling of complex structures as coupled sets of oscillators: Ensemble mean and variance of energy, J. Sound. Vib. 317(3-5) (2008) 760-780.

Journal Pre-proof

Declaration of interests

☒ The authors declare that they have no known competing financial interests or personal relationships that could have appeared to influence the work reported in this paper.

☐The authors declare the following financial interests/personal relationships which may be considered as potential competing interests:

Journal Pre-proof

Nicolas Totaro: Methodology, Software, Writing- Original draft, Writing- Reviewing and Editing

Jean-Louis Guyader: Conceptualization

Journal Pre-proof